Journal of Electrical and Computer Engineering Innovations
(JECEI)
Journal homepage: http://www.jecei.sru.ac.ir

Research paper

A SEPIC-Cuk-CSCCC Based SIMO Converter Design Using PSO-MPPT For Renewable Energy Application

S. Mukherjee*

Department of Electrical Engineering, RCC institute of information technology, Kolkata, India.

Article Info

Article History:
Received 06 December 2021
Reviewed 25 January 2022
Revised 27 February 2022
Accepted 13 March 2022

Keywords:
Particle swarm optimization - MPPT
SPV based application
Single input multiple outputs
DC-DC power conversion

*Corresponding Author's Email Address:
sarbo.1234@gmail.com

Abstract

Background and Objectives: The increasing requirement of different voltage and power levels in various power electronics applications, especially based on renewable energy, is escalating the growth of the different DC-DC converter topologies. Besides single-input single-output (SISO), multi-input multi-output (MIMO) type topologies become famous. So, in this paper, a Single-Ended Primary Inductance Converter (SEPIC), Cuk and Canonical Switch Cell (CSC) based single-input multi-output (SIMO) boost converter is proposed with a maximum power point tracking (MPPT) controller.
Methods: The Design of the three different DC-DC converter-based SIMO topology has been developed and thereafter the operation of the proposed converter is verified with Solar Photovoltaic (SPV), connected as an input to the converter. To extract maximum power from the SPV and MPPT controller is also developed. Finally, the converter's transfer function is developed using small-signal analysis and the system's stability is analyzed with and without compensation.
Results: A MATLAB simulation has been done to verify the theoretical analysis. Successful extraction of the maximum power from the SPV panel (65W, V_{mpp} 18.2V, I_{mpp} = 3.55A) with Particle Swarm Optimization (PSO) is verified. SEPIC and Cuk-based DC-DC converter can successfully operate in boost mode with a gain of 2.66. A significant reduction in the Cuk converter capacitor voltage ripple is also established.
Conclusion: So, this paper represents an SPV-fed SIMO boost converter based on SEPIC Cuk CSC topology. In addition to that, a PSO-based MPPT controller is also introduced for maximum power extraction. Verification of the theoretical analysis with simulation results is also described.

Introduction

To meet the growing power demand without any environmental issues, renewable energy sources are the most eligible option in the recent era. Continuous decrement of the Solar Photo Voltaic (SPV) cost makes itself more valuable for future research and implementation [1]. Besides that, the SPV system has the advantages of the absence of rotating parts, minimum maintenance, and almost zero environmental loss [2].

The power characteristics of the renewable energy source are nonlinear because of the dependency on solar irradiance, ambient temperature. The typical P-V and V-I characteristics of any solar photo-voltaic cell are shown in Fig. 1. There exists one operating point where they generate maximum power. To take full advantage of available energy resource and achieve maximum utilization efficiency, maximum power point tracking (MPPT) control techniques that extract maximum power from the renewable source is essential.

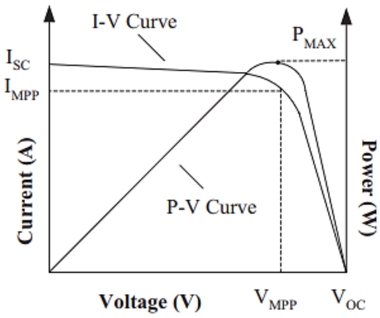

Fig. 1: Typical P-V and V-I characteristics of SPV cell [3].

Several researchers prescribed different MPPT methods for extracting maximum power [3]-[6]. Based on the involvement of several control variables, types of control strategies, nature of the available circuitry, and cost of applications are the main factors to select the MPPT algorithm. The PSO-based MPPT control method is one of the most effective techniques which can accurately track the maximum power point under variable ambient conditions. A swarm intelligence-based algorithm PSO is used to operate by finding the global optimal solution [7], [8]. The primary reason behind the popularity of this algorithm is the presence of very few numbers adjustable parameters.

The evolution of developing DC-DC converter has been constant over the past year. The requirement of different voltage and power levels across the power electronics devices in different applications enhances the growth of the development of the DC-DC converter. So not only the single quadrant converter, multi-level [9]-[11] and multi quadrant converter [12] has become famous day by day for their new control strategy and topologies, which cause the efficiency improvement and the reduction of size. In this paper [9], the advantage and disadvantages of several types of multi-output converter were described. It has been observed that the efficiency of the system is reduced if multiple active switches are used with high-frequency switching. Single input multiple output (SIMO) converter is one of the well-known multi-port converters used for such applications. i.e. Hybrid/ Electric Vehicles (EHV), microelectronics, lighting, telecommunication, channel multiplexing, and digital communication [13], [14], etc. This topology consists of a single inductor, responsible for controlling the current and voltage of different output ports. So, sometimes this topology is named “Single Inductor Multiple Output” (SIMO). Increased efficiency with reduced cost can be achieved in the SIMO converter as less number component is used.

In this paper, a SEPIC Cuk CSC combination converter-based SIMO converter, connected with an SPV, is proposed. A single switch is shared by all of these converters which provides simplification in control. A Particle Swarm Optimization (PSO) based MPPT control is implemented to extract maximum power from the SPV. In the proposed converter SEPIC converter provide positive voltage output. Besides this Cuk and CSC converter produced a negative output voltage. A simulation model is developed in MATLAB/Simulink software and the verification of PSO –MPPT based SIMO converter output is verified. So, implementation of the MPPT, simultaneous regulated bipolar voltage generation and minimum switching loss are the major advantages of the proposed converter.

The rest of the paper is organized as follows: the next section is named as a proposed converter which explains the construction of the proposed topology. The next section is named as an operational principle where the operation of the PSO-based MPPT controller and the different DC-DC converter is explained. In the next section, named as a design consideration, the selection of the inductor and capacitor is discussed. After that, the stability analysis and the effect of the controller in the proposed system are discussed. In the next section details of the simulation results are discussed along with the comparison of the proposed topology with other SIMO converters. Finally, the last section contains the conclusion of the proposed study.

Proposed Topology

In [15], [16], basic topologies of the non-isolated converter are introduced for solar PV application. Besides the conventional topologies, a combination of these converters can sometimes be found advantageous in many applications as given in [17]-[20].

A comparative study of different MPPT techniques for a basic converter with their performance analysis is also described in [4]. PSO-based MPPT algorithm is preferred over conventional techniques like perturb and observe (P and O) and incremental conductance (IC). In this paper, a SEPIC-Cuk-CSC combinational SIMO converter is proposed in Fig. 2, where a PSO-based MPPT technique is applied to extract maximum solar PV power.

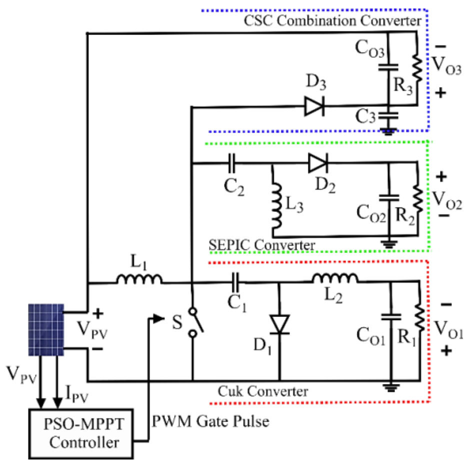

Fig. 2: Proposed SEPIC-Cuk-CSC Converter.

Operating Principal

A. PSO –MPPT Algorithm

Particle Swarm Optimization (PSO) is a population-based intelligence optimization technique, inspired by the foraging behaviour of a flock of birds and fish schooling in search of food. In PSO algorithm individual birds are referred to as individual flying particle that has their fitness value. Each particle's movement, in terms of direction and distance, ncy as calculated by the objective function and the velocity of the individual particle. Exchange of information between the particles happened based on their search process. P_{best} and G_{best} are the best position of the individual particle and the best position of all the particle, comparing all the P_{best} , respectively. All the swarm updates their direction and velocity to move towards the best position. So, convergence can be achieved [21]-[23]. The standard PSO algorithm can be represented by

$$v_i(k+1)=wv_i\left(k\right)+c_1r_1\left(P_{best}-x_i\left(k\right)\right)+c_2r_2\left(G_{best}-x_i\left(k\right)\right) \quad (1)$$

$$P_{best}=x_{ik} \quad (2)$$

$$f\left(x_{ik}\right)>f\left(P_{best,i}\right) \quad (3)$$

$$x_i(k+1)=x_i(k)+v_i(k+1) \quad (4)$$

where, $i=1,2.....N$. v_i and x_i are the velocity and the position of the particle i , the number of iteration denoted by k, w represents the inertia weight. r_1 and r_2 are the uniformly distributed random variable within [0 and 1]. Cognitive and social coefficients are denoted by c_1 and c_2 . P_{best} and G_{best} represent the individual best position of the i^{th} particle and the swarm best position of all the particle. If (5) is satisfied then the value of the P_{best} can be updated by (6).

$$f\left(x_{ik}\right)>f\left(P_{best,i}\right) \quad (5)$$

$$P_{best}=x_{ik} \quad (6)$$

where, f represents the objective function that should be maximized.

In Fig. 3, PSO-based MPPT topology is described. As given in the flowchart at the beginning particle swarm position and fitness value evaluation function are defined as the duty cycle and the generated output power respectively. A random initialization, within a uniform distribution, is made for the position and the velocity of each particle.

After that the fitness value of the particle is calculated, it is updated compared with the previous value. P_{best} and G_{best} of each particle are also updated against the previous values. Thereafter particle velocities and positions are updated accordingly.

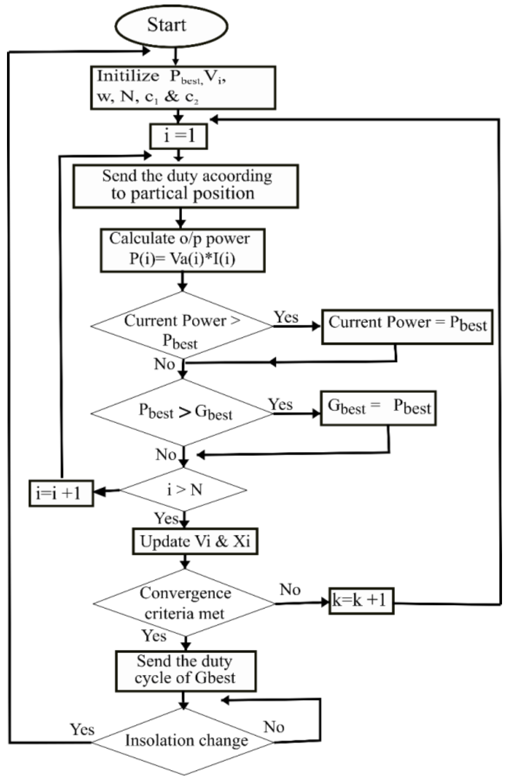

Fig. 3: PSO-based MPPT algorithm flowchart.

With the new values v_i and x_i, the convergence criteria are checked, which are either optimal solution localization or reaching the maximum number of iterations. Depending upon the weather condition and the load value, the fitness function becomes variable. So, the PSO must be reinitialized to search for a new MPP as the output of the PV module changes.

B. Single Input Multiple Output (SIMO Converter)

In this section, an interesting combination of SEPIC Cuk CSC combination converter topology is introduced. The ability to produce both positive and negative voltage simultaneously makes this converter topology suitable for renewable energy-based dc bipolar network applications. As given in Fig. 2 the CSC converter and Cuk converter produce a negative voltage whereas the SEPIC converter produces a positive voltage at the load output terminal.

C. SEPIC Converter

The Single-Ended Primary Inductance Converter or SEPIC converter is a modification of a non-isolated DC-DC converter. Some of the features, which makes this converter suitable for the PV application, are given by [24], [25] non-inverted output, the input inductor provides a low input ripple and noise, multiple inductors can be a couple in the same core, galvanic isolation can be easily obtained by replacing one of the inductors by a high-frequency transformer. The conventional SEPIC converter is shown in Fig. 4 where Vg is termed as an input dc voltage source. A MOSFET can be used as switch S, which is having a duty cycle of D.

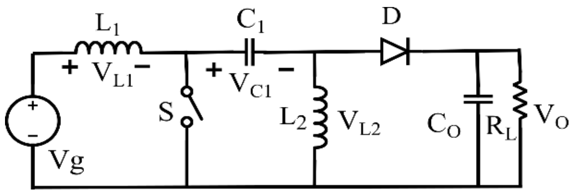

Fig. 4: SEPIC Converter topology.

In continuous conduction mode, the SEPIC converter operates in two different modes shown in Fig. 5a and Fig. 5b. In mode (a) when the switch S is turned on (duration is given by $0 \le t \le DT$, Where T represents the time period of the gate pulse), both the inductor current (I_{L1} and I_{L2}) is increasing because of charging and no energy is transferred to the load as D became reversed biased. In mode (b), when the switch S is turned off (duration given by $DT \le t \le T$), the D becomes forward biased and the energy is transferred to the load as both the inductor (I_{L1} and I_{L2}) are now discharging.

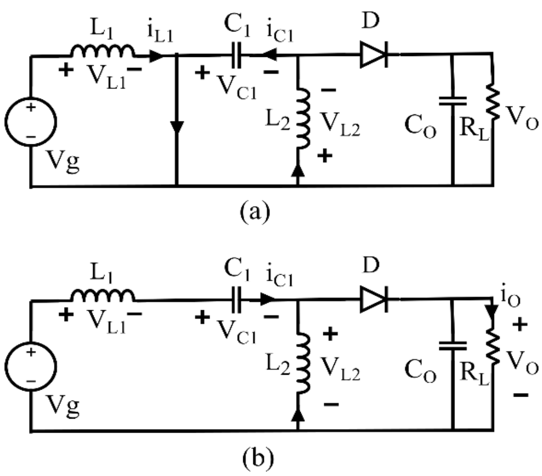

Fig. 5: Operation of SEPIC converter. (a) When S is turned on. (b) When S is turned off.

The volt-second balance across the inductor L_1 and L_2 given by

$$V_g DT + \left(V_g - V_{C1} - V_D - V_O\right)(1-D)T = 0 \tag{7}$$

$$V_{C1} DT + \left(-V_O - V_D\right)(1-D)T = 0 \tag{8}$$

where V_D represents the voltage drop across the diode.

The output of the SEPIC converter is represented as

$$V_O = \frac{DV_g}{(1-D)} \tag{9}$$

The value L_1, C_1 and L_2 of the SEPIC converter can be calculated by [26]

$$L_1 = \frac{V_g D}{\Delta I_{L1}.f_s} \tag{10}$$

$$L_2 = \frac{V_g D}{\Delta I_{L2}.f_s} \tag{11}$$

$$C_1 = \frac{V_O D}{R_L \Delta V_O f_s} \tag{12}$$

D. Cuk Converter

Cuk converter is a cascaded combination of the basic boost converter and buck converter with a coupling capacitor as described in [27]. The basic structure of the Cuk converter is given in Fig. 6. Energy is transferred from the input side to the output side through the coupling capacitor.

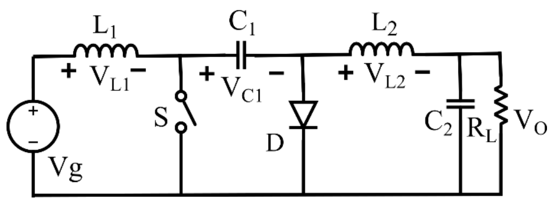

Fig. 6: Basic Cuk Converter Circuit.

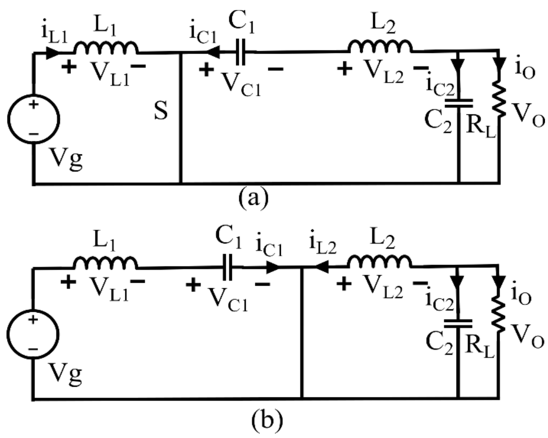

Fig. 7: Operation of Cuk Converter, (a) when S is turned on. (b) when S is turned off.

The features of the Cuk converter are stated as input and output current is continuous, low switching losses and higher efficiency, have low noise generation and low electromagnetic interference. As it is a combination of buck-boost dc-dc converter, it can able to deliver output voltage both greater and less than the input voltage. The operation of the Cuk converter can be divided into two modes (a) and (b) as shown in Fig. 7a and Fig. 7b respectively.

Mode (a) begins when the switch S is turned on (duration is given by $0 \le t \le DT$). At this mode current through the inductor L_1 increase as it is getting charged by the input voltage. On the other side C_1 is discharging through the output capacitor C_2 and the inductor L_2 by making diode D reverse biased. On the other mode (b) begins when switch S is turned off (duration is given by $DT \le t \le T$). In this mode diode, D became short-circuited which help the capacitor C_1 to get charged by the supplied voltage, and the inductor L_2 transfer the energy to the load by getting discharged. So, the coupling capacitor C_1 is transferring the energy from source to load by charging and discharging. The load voltage became negative as in both the mode the current flowing through the load is opposite in direction.

Applying volt-second balance across the inductor L_1,

$$V_g DT + (V_g - V_{C1})(1 - D)T = 0 \tag{13}$$

$$V_{C1} = \frac{V_g}{(1-D)} \tag{14}$$

Applying volt-second balance across the inductor L_2

$$(V_O + V_{C1})DT + V_O(1 - D)T = 0 \tag{15}$$

$$V_O = -\frac{DV_g}{(1 - D)} \tag{16}$$

Equation (16) represents the output of the Cuk converter. Applying the power balance, the value of the current I_{L1} given as

$$I_{L1} = \frac{D^2}{(1 - D)^2}\frac{V_g}{R_L} \tag{17}$$

Voltage ripple across the capacitor C_1 is calculated as

$$\Delta V_{C1} = \frac{D^2 V_g T}{R_L C_1 (1 - D)} \tag{18}$$

E. Canonical Switch Cell (CSC) Converter

CSC converter is a modification of a buck-boost converter with having fewer no of devices as shown in Fig. 8. The operation of the converter is divided into two different modes (a) and (b). At mode (a), as the switch S is turned on, the input inductor L_1 is getting charged from the source Vg. Simultaneously the capacitor C_1 discharges its stored energy to L_1 through the switch S, as the diode became reversed bias.

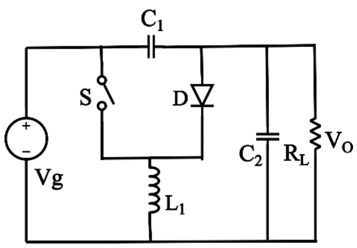

Fig. 8: CSC converter circuit.

Mode (b) begins when the switch S became turned off. Then the diode becomes forward biased and then the input inductor L_1 discharges its energy to the output capacitor C_2. Besides that, the capacitor C_1 is also getting charged by the input voltage through diode D, as shown in Fig. 9a and Fig. 9b.

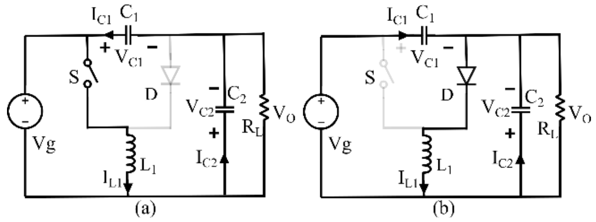

Fig. 9: Operation of CSC converter. (a) When S is turned on. (b) when S is turned off.

The expression of the capacitor C_1 and C_2 are calculated as [28]

$$C_1 = \frac{V_g D}{\Delta V_{C1} R_L f_s} \tag{19}$$

$$C_2 = \frac{I_O}{2\omega_L \Delta V_O} \tag{20}$$

where R_L represent the equivalent DC load resistance, ω_L represent the angular frequency of the line voltage.

Designing Consideration

A. Design of the inductor (L_1)

The inductor (L_1) is one of the primary components of this SIMO converter as the amount of energy transfer to the different output terminals is controlled by the energy stored in the inductor during the switch turned on time. The value of the inductor can be calculated from (10). It has been observed that the value of the inductor is depending on the duty cycle (D), the magnitude of the ripple current, and the input voltage. Considering the input voltage as a constant value, the variation of the inductance for the variation of the ripple current value (15% to 20%) and duty cycle (25% to 75%) is shown in Fig. 10.

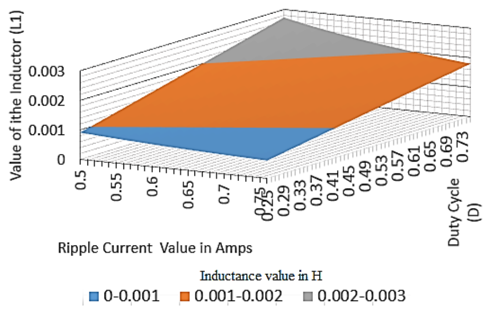

Fig. 10: Variation of the inductance (L_1) depending on the duty cycle and the ripple current values (in amps).

A variation of inductance value from 0.5mH to 2.7mH can be observed in Fig. 9. Besides that, as the panel output voltage is also changed depending on the ambient condition, the variation of the inductance value, with an assumption of constant ripple current and the variable duty cycle is plotted in Fig. 11.

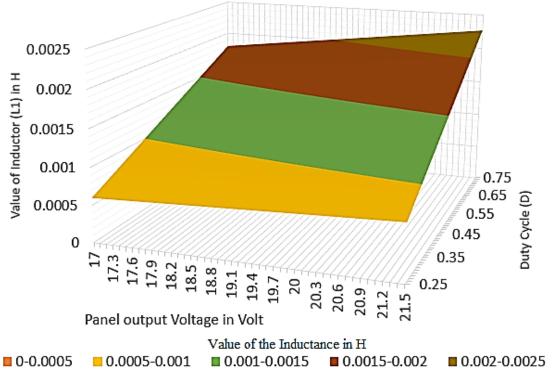

Fig. 11: Variation of the inductance (L_1) depending on the duty cycle and input voltage (in volt).

From Fig. 9 and Fig. 10, a value of 2.1mH is chosen as the value of the inductor L_1 after assuming the value of the ripple current is around 20%.

B. Design of the capacitor (C_1)

Similarly, the value of the capacitor (C_1) can also be calculated from (18).

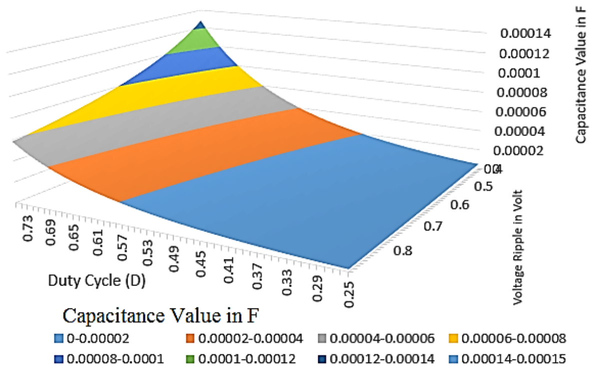

Fig. 12: Variation of the capacitance (C_1) depending on the duty cycle and ripple voltage values (in volt).

Initially considering the value of the load resistance 80Ω, the variation in the capacitance value depending on duty cycle (from 25% to 75%) and voltage ripple (.4V to .9V) is shown in Fig. 12.

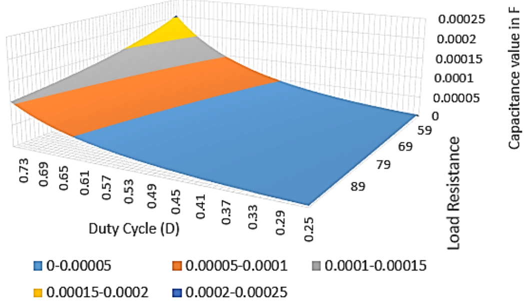

Fig. 13: Variation of the capacitance (C_1) depending on the duty cycle and Load resistance values (in ohm).

Besides, considering a constant ripple voltage of .4V, the variation of the capacitance value depending on the duty cycle (25% to 75%) and the load resistance (50 to 100) ohm is shown in Fig 13. So, after analyzing both Fig. 12 and Fig. 13, a capacitance value of 220µF is chosen as capacitance.

Stability Analysis and effect of Controller

As the SIMO converter is fed from the SPV supply, the primary purpose of the controller is to maintain a maximum power extraction from the SPV throughout the operation. Fig. 14 shows the block diagram of the proposed converter control system.

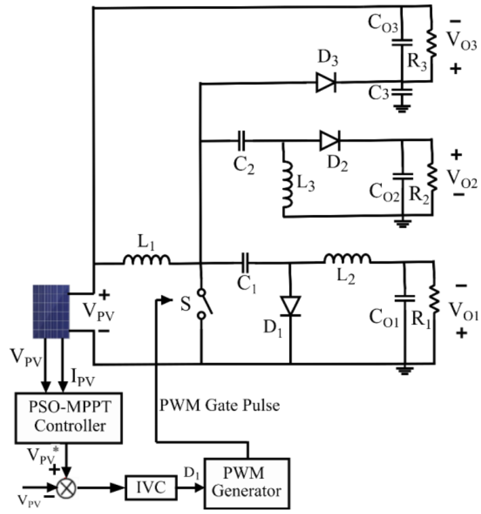

Fig. 14: Overall block diagram of total system.

A feed-forward controller consisting of an MPPT controller and an Input Voltage Controller (IVC) has been considered a total control system. After taking inputs (V_{PV} and I_{PV}) from the SPV panel, the MPPT controller develop a reference voltage V_{PV}^{*} with the help of the PSO algorithm. Then an error signal is generated after comparing the reference signal with the SPV output voltage. Thereafter this error signal is given as an input to the IVC and The signal D_1 is developed. An equivalent 10kHz PWM signal is generated by the PWM generator by taking the D_1 as an input.

The transfer function of the proposed converter is calculated with the help of small-signal modelling. After replacing the different component value the transfer function of the proposed converter is given by,

$$\mathrm{TF(s)} = \frac{-6.845s^3 - 2.252e^{04}s^2 - 4.33e^{05}s - 1.07e^{06}}{s^3 + 281.6s^2 + 4361s + 1.277e^{04}} \quad (21)$$

The position of the poles and zeros, as shown in Fig. 15, depicts that the stability of the system is marginal. The stability is further enhanced by shifting the position of the pole away from the imaginary axes by inserting a PID controller.

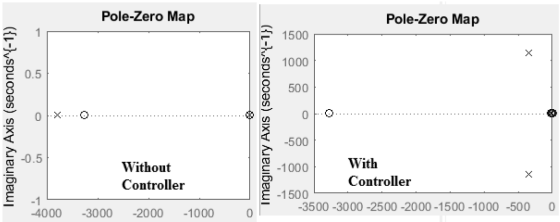

Fig. 15: Pole Zero Plot of the system with and without controller.

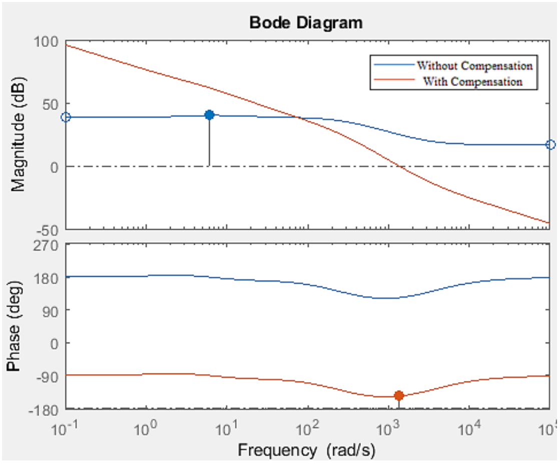

Fig. 16: Bode plot of the system with and without controller.

Similarly, improvement of the gain margin and the reduction in the gain cross-over frequency (GCF) is also achieved as shown in Fig. 16. Reduction of GCF defines a significant reduction of the system noise.

Further, the improvement of the stability of the compensated system can be observed from the nyquist plot as shown in Fig. 17. The reduction in the encirclement of the point (-1+j0) is observed after insertion of the controller.

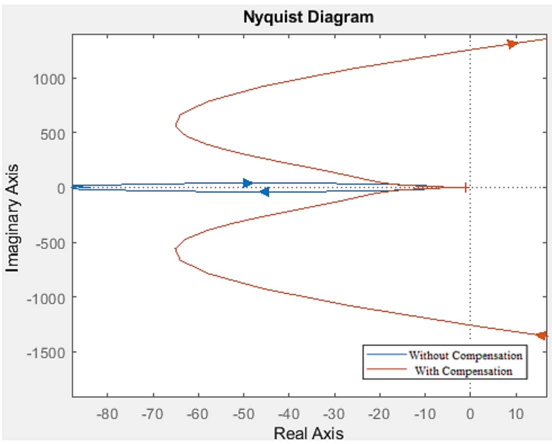

Fig. 17: Nyquist plot of the system with and without controller.

Simulation Results

To verify the PSO-MPPT based SEPIC-Cuk-CSC combinational converter characteristics, a simulation is performed in MATLAB as shown in Fig 13 the details of the SPV panel and the SIMO converter component specification, which is used in this simulation, is given in the Table 1.

Fig.18a shows the PWM gate pulse of 10 kHz developed by the PSO-MPPT. The SPV panel output voltage and the SPV panel extracted power are shown in Fig. 18b and Fig. 18c respectively. A swing of SPV voltage around the 18.2V (V_{mpp}) can be observed, which signifies a satisfactory execution of PSO-based MPPT.

Table 1: Component specification

	Name	Rating
Solar PV Panel	Input Panel Power	65W
	Open circuit Voltage (V_{oc})	22V
	The voltage at MPP (V_{mpp})	18.2V
	Short Circuit Current (I_{sc})	5.5A
	Current at MPP (I_{mpp})	3.55A
Reactance	Inductor L_1	2.1mH
	Inductor L_2 and L_3	1.35mH
	Capacitor C_1	220µF
	Capacitor C_2	470µF
	Resistance R_1-R_3	80Ω
	Switching Frequency	10kHz

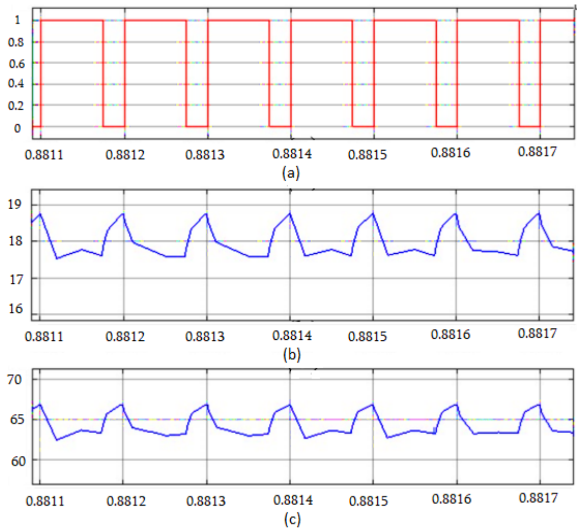

Fig. 18: (a) PWM output of the PSO-MPPT controller. (b) SPV panel output voltage (c) Solar PV panel output Power.

In Fig. 19b and Fig. 19d, the charging current of the inductor L_1 and the discharging current of the inductor L_2 are observed during the switch turn-on time. Besides that, the charging and the discharging of the capacitor C_1 are also shown in Fig. 19c.

Similarly, the charging and discharging of the capacitor C_2 along with the inductor L_3 of the SEPIC converter is shown in Fig. 20. It has been observed, in Fig. 20d, that a ripple of 0.5A is present in the inductor current. Different characteristics of the CSC converter are shown in Fig. 21. Where Fig. 21a and Fig. 21b represented the PWM gate pulse and the current characteristics of the inductor L_1.

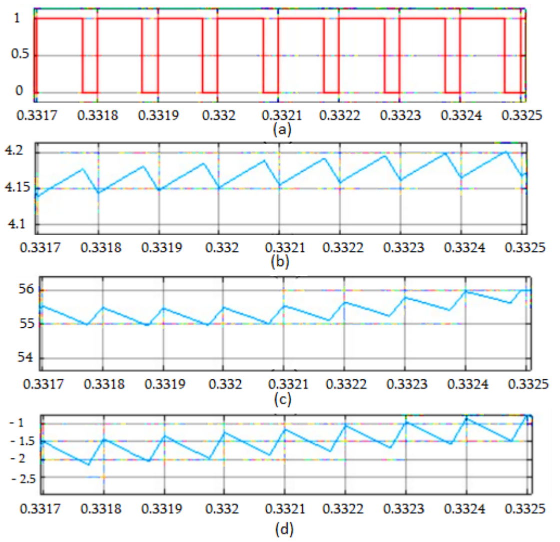

Fig. 19: Cuk converter output (a) PWM Gate pulse of switch S. (b) L1 inductor current. (c)The voltage across capacitor C1. (d) L2 inductor current.

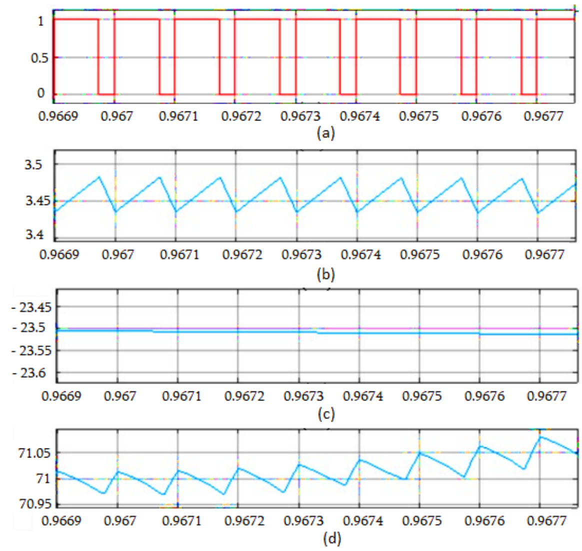

Fig. 21: CSC converter output. (a) PWM Gate pulse of switch S. (b) L1 inductor current. (c)The voltage across capacitor C_{O3}. (d) The voltage across capacitor C_3.

Charging and discharging of the capacitor C_3 is verified in Fig. 21d. The voltage across the capacitor C_{03} almost remains constant as it is shown in Fig. 21c. Continuous Mode of Conduction (CCM) operation is observed in the all of the converter.

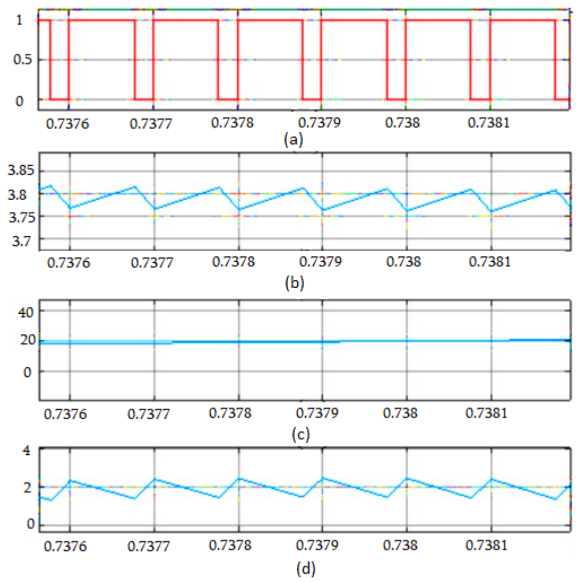

Fig. 20: SEPIC converter output (a) PWM Gate pulse of switch S. (b) L1 inductor current. (c) The voltage across capacitor C2. (d) L3 inductor current.

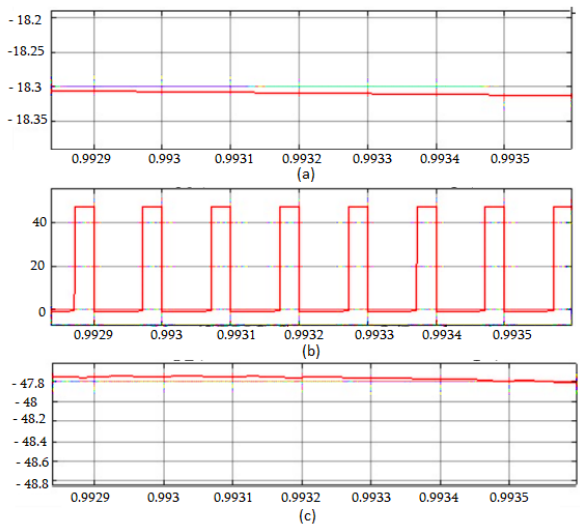

Fig. 22: Multiple output voltage of SIMO converter. (a) CSC converter output voltage. (b) SEPIC converter output voltage (c) Cuk Converter output voltage.

Three different voltage output with proper polarity is shown in Fig. 22. Where SEPIC and Cuk converter produces almost 48V and -48V with a gain of 2.6. Besides, the CSC converter is developing a voltage of around -18V.

A comparative analysis of the propose SIMO converter with some other SIMO converter is shown in Table 2.

In [29], the no of active and passive component used is much higher than other topologies. Besides that, the topology, proposed in [14], experienced a high switching loss as hard switching technique is used. MPPT control implementation is also not proposed in this topology. Though MPPT control was implemented in [30], but only two unipolar DC voltage is generated from this converter. So, comparing the proposed topology with the other proposed converter, the advantages can be summarized as (a) Implementation of MPPT, (b) Simultaneous generation of both positive and negative regulated voltage. (c) Minimum switching loss.

Table 2: Comparison with other SIMO topologies

Converter reference	[30]	[29]	[14]	Proposed Topology
Use of MPPT	Yes	No	No	Yes
No of Output	2	2	3	3
Output voltage polarity	Only positive	Only positive	Only Positive	Both Positive and Negative
Total No of Component	7	21	9	13
Inductor	1	1	1	3
Capacitor	2	8	3	6
Diode	2	7	0	3
Active Switch	2	2	5	1
Switching Loss	Medium	Medium	High	Low

Conclusion

This paper presents a design of the SEPIC-Cuk-CSC combination converter used for renewable energy applications. A PSO-based MPPT method is applied to extract maximum power. According to the simulation results, it is observed that the PSO method is successfully able to track the MPP in all the conditions. Reduction of design cost and loss is achieved by reducing the component requirement for developing multiple output voltage levels.

Conflict of Interest

The author declares that there is no conflict of interest regarding the publication of this manuscript. In addition, the ethical issues, including plagiarism, informed consent, misconduct, data fabrication and/or falsification, double publication and/or submission, and redundancy have been completely observed by the authors.

Abbreviations

SISO	Single Input Single Output
SIMO	Single Input Multiple Output
MIMO	Multiple input multiple Output
PSO	Particle Swarm Optimization.
MPPT	Maximum Power Point Tracking
P_{best}	Best position of the individual Particle
G_{best}	Best position among all the particles
v_i	The velocity of the particle
x_i	Position of the particle

References

[1] R.J. Wai, W.H. Wang, C.Y. Lin, "High-performance stand-alone photovoltaic generation system," IEEE Trans. Ind. Electron., 55(1): 240–250, 2008.

[2] M.M.A. Salama, M.Z. Shams El-Dein, M. Kazerani, "Optimal photovoltaic array recon fi guration to reduce partial shading losses," IEEE Trans. Sustain. Energy, 4(1): 145–153, 2013.

[3] A. Gupta, Y.K. Chauhan, R.K. Pachauri, "A comparative investigation of maximum power point tracking methods for solar PV system," Sol. Energy, 136: 236–253, 2016.

[4] B. Subudhi, R. Pradhan, "A comparative study on maximum power point tracking techniques for photovoltaic power systems," IEEE Trans. Sustain. Energy, 4(1): 89–98, 2013.

[5] M.A. Husain, Z.A. Khan, A. Tariq, "A novel solar PV MPPT scheme utilizing the difference between panel and atmospheric temperature," Renew. Energy Focus, 19–20(00): 11–22, 2017.

[6] A.K. Podder, N.K. Roy, H.R. Pota, "MPPT methods for solar PV systems: A critical review based on tracking nature," IET Renew. Power Gener., 13(10): 1615–1632, 2019.

[7] V. Phimmasone, Y. Kondo, T. Kamejima, M. Miyatake, "Verification of efficacy of the improved PSO-based MPPT controlling multiple photovoltaic arrays," in Proc. Int. Conf. Power Electron. Drive Syst.: 1015–1019, 201.

[8] K.K. Jha and M.N. Anwar, "Solar photovoltaic based brushless DC motor driven water pumping system using PSO-MPPT algorithm," in Proc. 2019 54th Int. Univ. Power Eng. Conf. (UPEC 2019): 1–6, 2019.

[9] E. Babaei, O. Abbasi, S. Sakhavati, "An overview of different topologies of multi-port dc/dc converters for dc renewable energy source applications," in Proc. 2016 13th Int. Conf. Electr. Eng. Comput. Telecommun. Inf. Technol. (ECTI-CON 2016), 2: 0–5, 2016.

[10] O. Ray, A.P. Josyula, S. Mishra, A. Joshi, "Integrated dual-output converter," IEEE Trans. Ind. Electron., vol. 62, no. 1, pp. 371–382, 2015, doi: 10.1109/TIE.2014.2327599.

[11] R. Lin, C.R. Pan, K.H. Liu "Family of single-inductor multi-output DC-DC converters," in Proc. 2009 International Conference on Power Electronics and Drive Systems (PEDS): 1216–1221, 2009.

[12] L. Cheng, F. Wang, "A new transformerless four quadrant DC-DC converter with wide conversion ratio," in Proc. 2021 IEEE Int. Conf. Power Electron. Comput. Appl. (ICPECA 2021): 486–491, 2021.

[13] H.F. Chinchero, J.M. Alonso, "Review on DC-DC SIMO converters with parallel configuration for LED lighting control," in Proc. 2020 IEEE Andescon, Andescon 2020, Quito, Ecuador, 2020.

[14] E. Agustianno, F.D. Murdianto, H.E.H. Suharyanto, "Design and simulation of single phase controlled full wave rectifier and simo buck converter for multi output power supply," in Proc. 2nd Int. Conf. Technol. Policy Electr. Power Energy, ICT-PEP 2020, 3: 312–316, 2020.

[15] F.D. Murdianto, M.Z. Efendi, R.E. Setiawan, A.S.L. Hermawan, "Comparison method of MPSO, FPA, and GWO algorithm in MPPT SEPIC converter under dynamic partial shading condition," in Proc. ICAMIMIA 2017 Int. Conf. Adv. Mechatronics, Intell. Manuf. Ind. Autom: 315–320, 2017.

[16] B.K. Panigrahi, P.R. Thakura, "Implementation of Cuk converter with MPPT," in Proc. 3rd IEEE Int. Conf. Adv. Electr. Electron. Information, Commun. Bio-Informatics, AEEICB 2017: 105–110, 2017.

[17] J. Chen, D. Maksimović, R. Erickson, "Buck-boost PWM converters having two independently controlled switches," in Proc. PESC Rec. - IEEE Annu. Power Electron. Spec. Conf., 2: 736–741, 2001.

[18] B. Lin, S. Member, F. Hsieh, "Soft-switching zeta – flyback converter with a buck – boost type of active clamp," IEEE Trans. Ind. Electron., 54(5): 2813–2822, 2007.

[19] K. Suresh et al., "A multifunctional non-isolated dual input-dual output converter for electric vehicle applications," IEEE Access, 9: 64445–64460, 2021.

[20] H. Aboreada, A.V.J.S. Praneeth, N. Vamanan, V. Sood, S.S. Williamson, "Design and control of non-isolated, multi-input dc/dc converter for effective energy management," IEEE Int.

Symp. Ind. Electron., 2019-June: 810–815, 2019.

[21] H. Renaudineau et al., “A PSO-based global MPPT technique for distributed PV power generation,” IEEE Trans. Ind. Electron., 62(2): 1047–1058, 2015.

[22] K. Ishaque, Z. Salam, M. Amjad, S. Mekhilef, “An improved particle swarm optimization (PSO)-based MPPT for PV with reduced steady-state oscillation,” IEEE Trans. Power Electron., 27(8): 3627–3638, 2012.

[23] M.A. Abdullah, T. Al-Hadhrami, C.W. Tan, A.H. Yatim, “Towards green energy for smart cities: Particle swarm optimization based MPPT approach,” IEEE Access, 6: 58427–58438, 2018.

[24] E. Durán, J. Galán, M. Sidrach-de-Cardona, J.M. Andújar, “A new application of the buck-boost-derived converters to obtain the I-V curve of photovoltaic modules,” in Proc. 2007 IEEE Power Electronics Specialists Conference: 413–417, 2007.

[25] J.J. Chacon, R.A. Ortiz, J.E. Archila, M.A. Mantilla, M.A. Botero, J.F. Petit, “Prototype for the characterization of photovoltaic panels based on a SEPIC converter,” in Proc. 2017 IEEE Workshop on Power Electronics and Power Quality Applications (PEPQA): 1–6, 2017.

[26] M.O. Ali, A.H. Ahmad, “Design, modelling and simulation of controlled sepic dc-dc converter-based genetic algorithm,” Int. J. Power Electron. Drive Syst., 11(4): 2116–2125, 2020.

[27] S. Chakrabarti, A.K. Panja, A. Mukherjee, A.K. Bar, Intelligent Electrical Systems: A Step towards Smarter Earth. CRC Press, 2021.

[28] V. Bist, B. Singh, “A PFC-Based BLDC motor drive using a canonical switching cell converter,” IEEE Trans. Ind. Informatics, 10(2): 1207–1215, 2014.

[29] M.Y. Hassani, M. Maalandish, S.H. Hosseini, “A new single-input multioutput interleaved high step-up DC-DC converter for sustainable energy applications,” IEEE Trans. Power Electron., 36(2): 1544–1552, 2021.

[30] V.S.K. Prasadarao, S. Peddapati, S.V.K. Naresh, “A single phase seven-level MLI with reduced number of switches employing a PV Fed SIMO DC-DC converter,” in Proc. 2020 IEEE Students’ Conf. Eng. Syst. SCES 2020, 2020.

Biographies

Sarbojit Mukherjee received his M.Tech degree from Calcutta University, Kolkata in 2011 and B.Tech degree in 2009, from the West Bengal University of Technology, Kolkata. Currently, he is working as an Assistant Professor in the Department of Electrical Engineering RCC Institute of Information Technology, Kolkata, India. He is currently pursuing her PhD at the Calcutta University, Kolkata, India. His research interest includes Power Electronics DC-DC Converter, Soft-Switched Converter and Electrical Drives.

- Email: sarbo.1234@gmail.com
- ORCID: 0000-0002-8893-3010
- Web of Science Researcher ID: ABA-7292-2022
- Scopus Author ID: 57219295564
- Homepage: NA

How to cite this paper:

S. Mukherjee, “A SEPIC-Cuk-CSCCC based SIMO converter design using PSO-MPPT for renewable energy application,” J. Electr. Comput. Eng. Innovations, 10(2): 437-446, 2022.

DOI: 10.22061/JECEI.2022.8379.509

URL: https://jecei.sru.ac.ir/article_1692.html